Predictive Current Control for Induction Motor Using Online Optimization Algorithm with Constrains

Zhiguo Wang[1], Zedong Zheng[1], Yongdong Li [1,2] , Boran Fan[1], Guibin Li[2]
[1] State Key Laboratory of Power System, Department of Electrical Engineering
Tsinghua University, Beijing, China
[2] Department of Electrical Engineering
Xinjiang University, Urumqi, Xinjiang, China
wzg13@mails.tsinghua.edu.cn, zzd@mail.tsinghua.edu.cn

***Abstract*—Model predictive control (MPC) has become a hot research topic in applications. The combination of continuous control set MPC (CCS-MPC) and pulse width modulation (PWM) can achieve high-performance while overcoming the drawback of the uncertain switching frequency of finite control set MPC (FCS-MPC). Based on the Field-oriented control (FOC), this paper proposes the CCS-MPC current control method by adopting the Hildreth's quadratic programming procedure. The proposed method applies the augmented model and realizes the unified offset-free control of the d-axes and q-axes currents with on-line optimization. Tuning weighting coefficients of cost function is the key to MPC design; based on analyzing the effect of the weighting coefficients and prediction horizon length on location of the closed-loop system poles, this study presents a new method to determine these parameters. Experimental results demonstrate that the CCS-MPC current control method has good dynamic features and decoupling characteristics.**

Keywords—CCS-MPC; predictive current control; offset-free control; Hildreth's quadratic programming procedure; weighting coefficients tuning

I. INTRODUCTION

Model predictive control (MPC) is becoming more and more popular due to its remarkable advantages over traditional control methods[1], such as easy handling of multivariable case, fast dynamic response, simple treatment of constraints, and easy inclusion of time variables and non-linearities.

MPC can be divided into CCS-MPC and FCS-MPC [1, 2]. CCS-MPC utilizes the motor model and cost functions, as well as analytical methods to obtain the optimal solutions of manipulated variables that can control power semiconductor devices with the modulator. Depends on the nature of power converter that combinations of switching states are finite, FCS-MPC uses complete enumeration method to achieve prediction and optimization, and the use of modulator is avoided [3]. Therefore, FCS-MPC is a kind of simplified MPC [4].CCS-MPC and FCS-MPC have similar dynamic features, but CCS-MPC has higher steady-state precision and smaller current ripples and determined switching frequency, which can ensure high-performance control of torque and speed[5]. This paper mainly studies predictive current control methods for the induction motor (IM) based on CCS-MPC.

CCS-MPC often uses methods such as simple amplitude limitation, explicit MPC (EMPC) and online optimization [6] to deal with the constraints. Amplitude limitation is easy to implement, but can only be used for simple independent constraints. EMPC [4, 7, 8] transfers a quadratic programming (QP) into a multi-parametric quadratic programming (mp-QP) by treating states variables as a parameter vector and obtains the explicit optimal solutions by solving this mp-QP problem. However, EMPC requires that the controlled object is a linear constant system, and the constraints are linear constraints [9]. The online optimization algorithm is more complex, requiring a large amount of calculation, but can handle time-varying systems and different types of constraints. This paper uses the Hildreth's QP procedure to realize the online optimization.

The prediction horizon length and weighting coefficients, which have no standard tuning methods now, are chosen by experiments or experience usually[2, 10].This paper proposes the method of determining the prediction horizon length and weighting coefficients according to the locations of the poles of the closed-loop system.

This paper is organized as follows. Section II introduces the mathematical analysis of CCS-MPC for current control of IM. Section III discusses the tuning method for prediction horizon length and weighting coefficients. Section IV presents experimental results.

II. CCS-MPC FOR CURRENT CONTROL OF IM

A. Augmented model of IM

In order to introduce integral links in the model, the augmented model in discrete-time form is adopted in this paper [6, 11]. The rotor speed ω_r can be approximately constant when the sampling frequency is high. In addition, the rotor flux Ψ_r can also be approximately constant because the sampling period is much smaller than the rotor time constant ($T_s << \tau_r$). Therefore, the terms related to rotor flux are eliminated in the

augmented model of IM. The augmented model is expressed as:

$$\begin{cases} \boldsymbol{x}_{\mathrm{a}}(k+1)=\boldsymbol{A}_{\mathrm{ad}}\boldsymbol{x}_{\mathrm{a}}(k)+\boldsymbol{B}_{\mathrm{ad}}\Delta\boldsymbol{u}(k) \\ \boldsymbol{y}_{\mathrm{a}}(k)=\boldsymbol{C}_{\mathrm{ad}}\boldsymbol{x}_{\mathrm{a}}(k) \end{cases} \tag{1}$$

where $\boldsymbol{x}_{\mathrm{a}}=\begin{bmatrix}\Delta i_{\mathrm{sd}} & \Delta i_{\mathrm{sq}} & i_{\mathrm{sd}} & i_{\mathrm{sq}}\end{bmatrix}^{\mathrm{T}}$ is for state vector, $\Delta\boldsymbol{u}=\begin{bmatrix}\Delta u_{\mathrm{sd}} & \Delta u_{\mathrm{sq}}\end{bmatrix}^{\mathrm{T}}$ is for input vector in form of increment, $\boldsymbol{y}_{\mathrm{a}}=\begin{bmatrix}i_{\mathrm{sd}} & i_{\mathrm{sq}}\end{bmatrix}^{\mathrm{T}}$ is for output vector.

The state matrix $\boldsymbol{A}_{\mathrm{ad}}$, the input matrix $\boldsymbol{B}_{\mathrm{ad}}$ and the output matrix $\boldsymbol{C}_{\mathrm{ad}}$ of the augmented model have the form of

$$\boldsymbol{A}_{\mathrm{ad}}=\begin{bmatrix} 1-\dfrac{1}{\sigma L_{\mathrm{s}}}\left(R_{\mathrm{s}}+\dfrac{L_{\mathrm{m}}^2}{L_{\mathrm{r}}^2}\cdot R_{\mathrm{r}}\right)T_{\mathrm{s}} & T_{\mathrm{s}}\omega_{\mathrm{s}} & 0 & 0 \\ -T_{\mathrm{s}}\omega_{\mathrm{s}} & 1-\dfrac{1}{\sigma L_{\mathrm{s}}}\left(R_{\mathrm{s}}+\dfrac{L_{\mathrm{m}}^2}{L_{\mathrm{r}}^2}\cdot R_{\mathrm{r}}\right)T_{\mathrm{s}} & 0 & 0 \\ 1-\dfrac{1}{\sigma L_{\mathrm{s}}}\left(R_{\mathrm{s}}+\dfrac{L_{\mathrm{m}}^2}{L_{\mathrm{r}}^2}\cdot R_{\mathrm{r}}\right)T_{\mathrm{s}} & T_{\mathrm{s}}\omega_{\mathrm{s}} & 1 & 0 \\ -T_{\mathrm{s}}\omega_{\mathrm{s}} & 1-\dfrac{1}{\sigma L_{\mathrm{s}}}\left(R_{\mathrm{s}}+\dfrac{L_{\mathrm{m}}^2}{L_{\mathrm{r}}^2}\cdot R_{\mathrm{r}}\right)T_{\mathrm{s}} & 0 & 1 \end{bmatrix},$$

$$\boldsymbol{B}_{\mathrm{ad}}=\begin{bmatrix} \dfrac{T_{\mathrm{s}}}{\sigma L_{\mathrm{s}}} & 0 & \dfrac{T_{\mathrm{s}}}{\sigma L_{\mathrm{s}}} & 0 \\ 0 & \dfrac{T_{\mathrm{s}}}{\sigma L_{\mathrm{s}}} & 0 & \dfrac{T_{\mathrm{s}}}{\sigma L_{\mathrm{s}}} \end{bmatrix}^{\mathrm{T}},\ \boldsymbol{C}_{\mathrm{ad}}=\begin{bmatrix}0&0&1&0\\0&0&0&1\end{bmatrix}.$$

where R_{s} and L_{s} are the stator resistance and inductance, R_{r} and L_{r} are the rotor resistance and inductance respectively, L_{m} is the mutual machine inductance, $\sigma=1-L_{\mathrm{m}}^2/L_{\mathrm{s}}L_{\mathrm{r}}$ is the leakage coefficient, ω_{s} is the synchronous angular frequency, T_{s} is the sampling period.

B. Prediction

The predictive formula for state variables and output variables can be obtained from the augmented model (1) is expressed as (2).

$$\begin{cases} \boldsymbol{X}_{\mathrm{a}}=\boldsymbol{F}_{\mathrm{a}}\boldsymbol{x}_{\mathrm{a}}(k)+\boldsymbol{\Phi}_{\mathrm{a}}\Delta\boldsymbol{U} \\ \boldsymbol{Y}_{\mathrm{a}}=\boldsymbol{F}_{\mathrm{aY}}\boldsymbol{x}_{\mathrm{a}}(k)+\boldsymbol{\Phi}_{\mathrm{aY}}\Delta\boldsymbol{U} \end{cases} \tag{2}$$

where N_{p} is prediction horizon length. The definitions of $\boldsymbol{X}_{\mathrm{a}}$, $\boldsymbol{Y}_{\mathrm{a}}$, $\boldsymbol{F}_{\mathrm{a}}$, $\boldsymbol{F}_{\mathrm{aY}}$, $\boldsymbol{\Phi}_{\mathrm{a}}$, $\Delta\boldsymbol{U}$ and $\boldsymbol{\Phi}_{\mathrm{aY}}$ are as follow.

$$\boldsymbol{X}_{\mathrm{a}}=\begin{bmatrix}\boldsymbol{x}_{\mathrm{a}}(k+1|k)\\ \boldsymbol{x}_{\mathrm{a}}(k+2|k)\\ \vdots\\ \boldsymbol{x}_{\mathrm{a}}(k+N_{\mathrm{p}}|k)\end{bmatrix},\ \boldsymbol{Y}_{\mathrm{a}}=\begin{bmatrix}\boldsymbol{y}_{\mathrm{a}}(k+1|k)\\ \boldsymbol{y}_{\mathrm{a}}(k+2|k)\\ \vdots\\ \boldsymbol{y}_{\mathrm{a}}(k+N_{\mathrm{p}}|k)\end{bmatrix},\ \boldsymbol{F}_{\mathrm{a}}=\begin{bmatrix}\boldsymbol{A}_{\mathrm{ad}}\\ \boldsymbol{A}_{\mathrm{ad}}^2\\ \vdots\\ \boldsymbol{A}_{\mathrm{ad}}^{N_{\mathrm{p}}}\end{bmatrix},$$

$$\boldsymbol{F}_{\mathrm{aY}}=\begin{bmatrix}\boldsymbol{C}_{\mathrm{ad}}\boldsymbol{A}_{\mathrm{ad}}\\ \boldsymbol{C}_{\mathrm{ad}}\boldsymbol{A}_{\mathrm{ad}}^2\\ \vdots\\ \boldsymbol{C}_{\mathrm{ad}}\boldsymbol{A}_{\mathrm{ad}}^{N_{\mathrm{p}}}\end{bmatrix},\ \boldsymbol{\Phi}_{\mathrm{a}}=\begin{bmatrix}\boldsymbol{B}_{\mathrm{ad}} & \boldsymbol{0} & \cdots & \boldsymbol{0}\\ \boldsymbol{A}_{\mathrm{ad}}\boldsymbol{B}_{\mathrm{ad}} & \boldsymbol{B}_{\mathrm{ad}} & \cdots & \boldsymbol{0}\\ \vdots & \vdots & \ddots & \boldsymbol{0}\\ \boldsymbol{A}_{\mathrm{ad}}^{N_{\mathrm{p}}-1}\boldsymbol{B}_{\mathrm{ad}} & \boldsymbol{A}_{\mathrm{ad}}^{N_{\mathrm{p}}-2}\boldsymbol{B}_{\mathrm{ad}} & \cdots & \boldsymbol{B}_{\mathrm{ad}}\end{bmatrix},$$

$$\boldsymbol{\Phi}_{\mathrm{aY}}=\begin{bmatrix}\boldsymbol{C}_{\mathrm{ad}}\boldsymbol{B}_{\mathrm{ad}} & \boldsymbol{0} & \cdots & \boldsymbol{0}\\ \boldsymbol{C}_{\mathrm{ad}}\boldsymbol{A}_{\mathrm{ad}}\boldsymbol{B}_{\mathrm{ad}} & \boldsymbol{C}_{\mathrm{ad}}\boldsymbol{B}_{\mathrm{ad}} & \cdots & \boldsymbol{0}\\ \vdots & \vdots & \ddots & \boldsymbol{0}\\ \boldsymbol{C}_{\mathrm{ad}}\boldsymbol{A}_{\mathrm{ad}}^{N_{\mathrm{p}}-1}\boldsymbol{B}_{\mathrm{ad}} & \boldsymbol{C}_{\mathrm{ad}}\boldsymbol{A}_{\mathrm{ad}}^{N_{\mathrm{p}}-1}\boldsymbol{B}_{\mathrm{ad}} & \cdots & \boldsymbol{C}_{\mathrm{ad}}\boldsymbol{B}_{\mathrm{ad}}\end{bmatrix},$$

$$\Delta\boldsymbol{U}=\begin{bmatrix}\Delta\boldsymbol{u}(k)\\ \Delta\boldsymbol{u}(k+1)\\ \vdots\\ \Delta\boldsymbol{u}(k+N_{\mathrm{p}}-1)\end{bmatrix}.$$

C. Cost function and receding optimization

In this paper, the quadratic form of cost function is adopted, expressed as (3).

$$J=\left[\boldsymbol{R}_{\mathrm{Y}}-\boldsymbol{Y}_{\mathrm{a}}\right]^{\mathrm{T}}\boldsymbol{Q}\left[\boldsymbol{R}_{\mathrm{Y}}-\boldsymbol{Y}_{\mathrm{a}}\right]+\Delta\boldsymbol{U}^{\mathrm{T}}\boldsymbol{R}\Delta\boldsymbol{U} \tag{3}$$

where, $\boldsymbol{Q}$ and $\boldsymbol{R}$ are weighting matrixes for current errors and voltage increment amplitudes. $\boldsymbol{R}_{\mathrm{Y}}$ is vector of reference values for d-axis and q-axis current. The definition of $\boldsymbol{Q}$, $\boldsymbol{R}$ and $\boldsymbol{R}_{\mathrm{Y}}$ are as follows.

$$\boldsymbol{Q}=\begin{bmatrix}\boldsymbol{Q}_1 & \boldsymbol{0} & \cdots & \boldsymbol{0}\\ \boldsymbol{0} & \boldsymbol{Q}_2 & \cdots & \boldsymbol{0}\\ \vdots & \vdots & \ddots & \boldsymbol{0}\\ \boldsymbol{0} & \boldsymbol{0} & \cdots & \boldsymbol{Q}_{\mathrm{N_p}}\end{bmatrix},\ \boldsymbol{R}=\begin{bmatrix}\boldsymbol{R}_1 & \boldsymbol{0} & \cdots & \boldsymbol{0}\\ \boldsymbol{0} & \boldsymbol{R}_2 & \cdots & \boldsymbol{0}\\ \vdots & \vdots & \ddots & \boldsymbol{0}\\ \boldsymbol{0} & \boldsymbol{0} & \cdots & \boldsymbol{R}_{\mathrm{N_p}}\end{bmatrix},$$

$$\boldsymbol{Q}_{\mathrm{i}}=\begin{bmatrix}q_{\mathrm{d\_i}} & 0\\ 0 & q_{\mathrm{q\_i}}\end{bmatrix},\ \boldsymbol{R}_{\mathrm{i}}=\begin{bmatrix}r_{\mathrm{d\_i}} & 0\\ 0 & r_{\mathrm{q\_i}}\end{bmatrix},$$

$$\boldsymbol{R}_{\mathrm{Y}}=\begin{bmatrix}\boldsymbol{R}^*(k+1)\\ \boldsymbol{R}^*(k+2)\\ \vdots\\ \boldsymbol{R}^*(k+N_{\mathrm{p}})\end{bmatrix},\ \boldsymbol{R}^*(k+i)=\begin{bmatrix}i_{\mathrm{sd}}^*(k+i)\\ i_{\mathrm{sq}}^*(k+i)\end{bmatrix}.$$

D. Constraints

In electric drives, the inverter can quickly generate the voltages for the motor, but d-axis and q-axis voltage amplitudes are constrained by bus voltage. Thus, the paper mainly considers the constraints on voltage amplitude which can be represented by (4) that are nonlinear and not easy to deal with. Thus, it needs linear constraints to approximate (4).

$$\sqrt{u_{\mathrm{sd}}^2+u_{\mathrm{sq}}^2}\le\frac{V_{\mathrm{DC}}}{\sqrt{3}} \tag{4}$$

The incremental form of discrete linear constraints of the input variables can be expressed by (5) where matrix $\boldsymbol{L}$ is a linear transformation matrix of input variables.

$$\boldsymbol{L}\Delta\boldsymbol{u}(k)+\boldsymbol{L}\boldsymbol{u}(k-1)\le\boldsymbol{\chi}(k) \tag{5}$$

The amplitude constraint formula of input variables in the incremental form is expressed as (6).

$$\boldsymbol{M}\Delta\boldsymbol{U}\le\boldsymbol{\gamma} \tag{6}$$

where

$$\boldsymbol{M}=\begin{bmatrix}\boldsymbol{L}&\boldsymbol{0}&\boldsymbol{0}&\cdots&\boldsymbol{0}\\ \boldsymbol{L}&\boldsymbol{L}&\boldsymbol{0}&\cdots&\boldsymbol{0}\\ \boldsymbol{L}&\boldsymbol{L}&\boldsymbol{L}&\cdots&\boldsymbol{0}\\ \vdots&\vdots&\vdots&\ddots&\vdots\\ \boldsymbol{L}&\boldsymbol{L}&\boldsymbol{L}&\cdots&\boldsymbol{L}\end{bmatrix},\ \boldsymbol{\gamma}=\begin{bmatrix}\boldsymbol{\chi}(k)\\ \boldsymbol{\chi}(k+1)\\ \boldsymbol{\chi}(k+2)\\ \vdots\\ \boldsymbol{\chi}(k+N_{\mathrm{c}}-1)\end{bmatrix}-\begin{bmatrix}\boldsymbol{L}\\ \boldsymbol{L}\\ \boldsymbol{L}\\ \vdots\\ \boldsymbol{L}\end{bmatrix}\boldsymbol{u}(k-1).$$

If using the hexagonal approximated circular constraints, $\boldsymbol{L}$ and $\boldsymbol{\chi}(k)$ can be represented as (7).

$$\begin{cases}\boldsymbol{L}=\begin{bmatrix}\frac{\sqrt{3}}{3}&-\frac{\sqrt{3}}{3}&-1&-\frac{\sqrt{3}}{3}&\frac{\sqrt{3}}{3}&1\\ 1&1&0&-1&-1&0\end{bmatrix}^{\mathrm{T}}\\ \boldsymbol{\chi}(k)=V_{\mathrm{DC}}\begin{bmatrix}\frac{2}{3}&\frac{2}{3}&\frac{1}{\sqrt{3}}&\frac{2}{3}&\frac{2}{3}&\frac{1}{\sqrt{3}}\end{bmatrix}^{\mathrm{T}}\end{cases} \tag{7}$$

E. Online optimization based on Hildreth's QP procedure

When the constraints are not considered, the optimal solution of input variables $\Delta\boldsymbol{U}$ can be derived by first derivation of cost function (3), which is expressed as (8).

$$\Delta\boldsymbol{U}=\boldsymbol{H}^{-1}\boldsymbol{F} \tag{8}$$

where $\boldsymbol{H}=\boldsymbol{\Phi}_{\mathrm{aY}}^{\mathrm{T}}\boldsymbol{Q}\boldsymbol{\Phi}_{\mathrm{aY}}+\boldsymbol{R}$, $\boldsymbol{F}=\boldsymbol{\Phi}_{\mathrm{aY}}^{\mathrm{T}}\boldsymbol{Q}\left[\boldsymbol{R}_{\mathrm{aY}}-\boldsymbol{F}_{\mathrm{aY}}\boldsymbol{x}_{\mathrm{a}}(k)\right]$.

Considering constraints, the optimal solution is expressed as (9).

$$\begin{cases}\boldsymbol{\lambda}_{\mathrm{act}}=-\left(\boldsymbol{M}_{\mathrm{act}}\boldsymbol{H}^{-1}\boldsymbol{M}_{\mathrm{act}}^{\mathrm{T}}\right)^{-1}\left(\boldsymbol{\gamma}_{\mathrm{act}}+\boldsymbol{M}_{\mathrm{act}}\boldsymbol{H}^{-1}\boldsymbol{F}\right)\\ \Delta\boldsymbol{U}=\boldsymbol{H}^{-1}\boldsymbol{F}-\boldsymbol{H}^{-1}\boldsymbol{M}_{\mathrm{act}}^{\mathrm{T}}\boldsymbol{\lambda}_{\mathrm{act}}\end{cases} \tag{9}$$

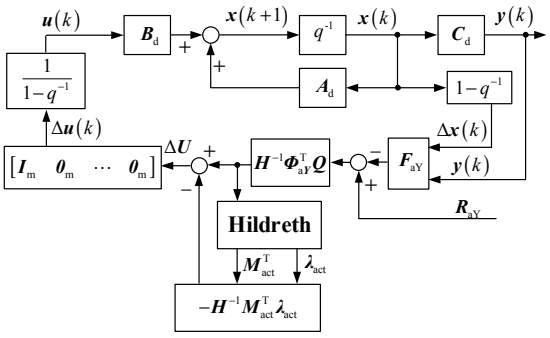

Fig. 1 CCS-MPC schematic using Hildreth's QP procedure

where $\boldsymbol{M}_{\mathrm{act}}$ and $\boldsymbol{\lambda}_{\mathrm{act}}$ are inequality coefficient matrix and Lagrange multiplier respectively which correspond to the active constraints.

Hildreth's QP procedure [6, 11, 12] gets the active constraints by solving the dual problem, and the method can be expressed as:

$$\begin{cases}\lambda_i^{m+1}=\max\left(0,\omega_i^{m+1}\right)\\ \omega_i^{m+1}=-\frac{1}{w_{ii}}\left[k_i+\sum_{j=1}^{i-1}w_{ij}\lambda_j^{m+1}+\sum_{j=i+1}^{n}w_{ij}\lambda_j^{m}\right]\end{cases} \tag{10}$$

where w_{ij} is the element corresponding to the subscript $ijth$ in the matrix $\boldsymbol{W}=\boldsymbol{M}\boldsymbol{H}^{-1}\boldsymbol{M}^{\mathrm{T}}$, and k_i is the element corresponding to the subscript ith in the vector $\boldsymbol{K}=\boldsymbol{\gamma}+\boldsymbol{M}\boldsymbol{H}^{-1}\boldsymbol{F}$.

The CCS-MPC based on Hildreth's QP procedure is presented in Fig. 1.

III. TUNING METHOD FOR PREDICTION HORIZON LENGTH AND WEIGHTING COEFFICIENTS

The effect of weighting matrix $\boldsymbol{Q}$ and $\boldsymbol{R}$ on the performance of CCS-MPC is decided by their ratio, so the elements in matrix $\boldsymbol{Q}$ are set to one, i.e. $q_{\mathrm{d\_1}}=q_{\mathrm{q\_1}}\cdots=q_{\mathrm{d\_N_p}}=q_{\mathrm{q\_N_p}}=1$. To simplify analysis, the elements in matrix $\boldsymbol{R}$ is set as $r_{\mathrm{d\_1}}=r_{\mathrm{q\_1}}\cdots=r_{\mathrm{d\_N_p}}=r_{\mathrm{q\_N_p}}=r$.

The effects of N_{p}, $\boldsymbol{Q}$ and $\boldsymbol{R}$ on the closed-loop system poles are presented in Fig. 2.

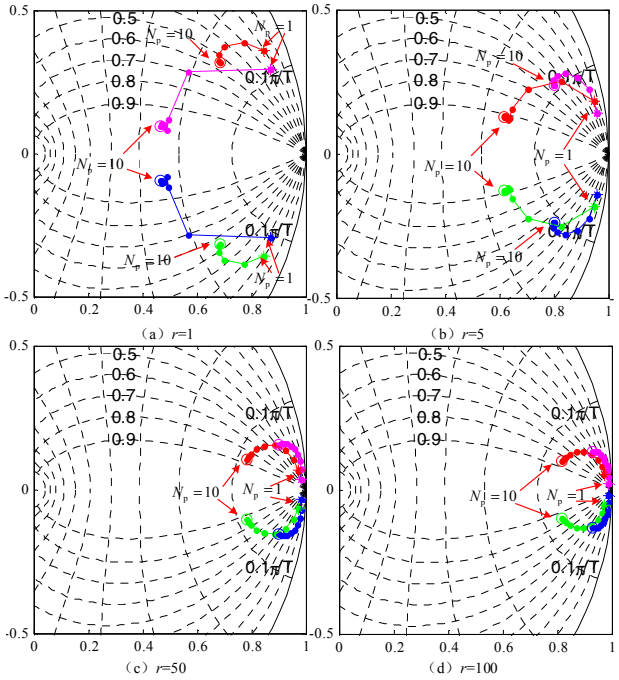

Fig. 2. The effects of N_{p}, $\boldsymbol{Q}$ and $\boldsymbol{R}$ on the closed-loop system poles

The value of r is set to 1, 5, 50, 100, and N_p changes from 1 to 10. When r is small, the poles are closer to the center of the unit circle and greater value of N_p has a little effect on the poles (when r=1 and N_p>4, the poles almost have no changes). On the contrary, when r is large, the poles are closer to the unit circle and greater value of N_p has the obvious effect on the poles (when r=50 and N_p>8, the poles almost have no changes). When the value of r is constant, the damping coefficient of the closed-loop system can be increased by increasing N_p within a proper range.

The value of N_p, $\boldsymbol{Q}$ and $\boldsymbol{R}$ are set as (11) so that the closed-loop poles keep a certain distance from the unit circle, which can ensure the system has a certain stability margin. At the same time, the damping coefficient of the closed-loop system is 0.71, which makes the system has good dynamic characteristics.

$$\begin{cases} N_p = 6 \\ \boldsymbol{Q} = \mathrm{diag}\begin{pmatrix} 1 & \cdots & 1 \end{pmatrix}_{12\times 12} \\ \boldsymbol{R} = \mathrm{diag}\begin{pmatrix} 11 & \cdots & 11 \end{pmatrix}_{12\times 12} \end{cases} \tag{11}$$

IV. Experiment Results

The proposed control strategy was studied on a 2.2-kW induction motor experimental system. The experiment adopts vector control algorithm as shown in Fig.3. The experiment system consists of inverter, controller and motor test rig as shown in Fig.4.

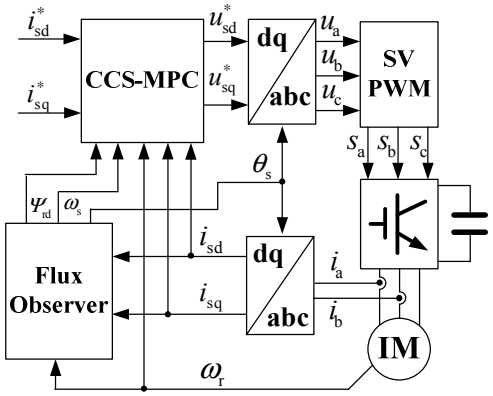

Fig.3. Vector control principle with CCS-MPC

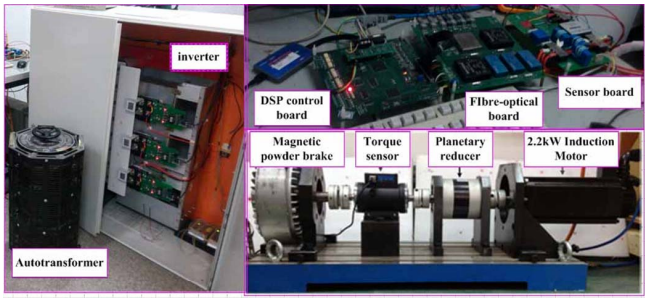

Fig. 4. Experimental system for IM

TABLE I. Parameters of the IM used in simulation and experiment

Parameter		Value
rated power	P_N	2.2 kW
rated frequency	f_N	50 Hz
rated voltage	U_N	380 V
rated current	I_N	5.3 A
number of pole pairs	N_p	2
stator resistance	R_s	1.97Ω
rotor resistance	R_r	2.34Ω
stator inductance	L_s	281.2mH
rotor inductance	L_r	281.2mH
mutual inductance	L_m	270mH

The controller uses 32-bit DSP chip TMS320F28335, which supports floating-point calculations, and its control cycle is 0.2ms. The driving signals to IGBT are generated by the DSP and are transmitted through the optical fiber to the IGBT driving circuit. The bus voltage of the inverter and the stator currents are measured by one voltage sensor (LV25 by LEM) and two current sensors (LA55 by LEM) respectively. The measured signals are sent directly to the control board. The inverter is a two-level type, which consists of three IGBT modules. Parameters of the IM used in the experiment are presented in Table I. The control cycle is 0.2ms.

A. Algorithm calculation load

Since the CCS-MPC presented in this paper uses the time-varying model, it is necessary to update $\boldsymbol{A}_{ad}$ $\boldsymbol{F}_{aY}$ $\boldsymbol{\Phi}_{aY}$ $\boldsymbol{H}^{-1}$ in real time and realize the Hildreth's QP procedure by an iterative search algorithm. Therefore, the computational complexity of the proposed CCS-MPC is much larger than that using a constant model.

Compared with other time matrices, the analytic solution of $\boldsymbol{H}^{-1}$ is difficult to obtain because of the inverse of higher-order symbolic matrices. Therefore, the $\boldsymbol{H}^{-1}$ matrix is obtained by off-line numerical calculation, and the numerical calculation is implemented by quadratic function fitting of ω_s. The matrices of $\boldsymbol{F}$ $\boldsymbol{W}$ and $\boldsymbol{K}$ can be updated by multiplication and addition. The total time for computing $\boldsymbol{H}^{-1}\boldsymbol{F}$ is about 10.6μs. The Hildreth's QP procedure requires 22μs to complete a search loop.

For the control cycle 200μs, the real-time update calculation and the 7 iteration search can be completed, which can basically guarantee the search convergence. When the number of iterations needs to be increased to ensure the search convergence and improve the search accuracy, the control frequency needs to be reduced.

B. Torque control mode

Fig.5 presents the d-axis and q-axis currents waveform when q-axis current has a step change in torque control mode. The motor started with 0.597(p.u.) d-axis excitation current. And then, q-axis current steps between 0.1(p.u.) and 1.0(p.u.).

The current ripple of d-axis and q-axis will increase when the speed rises. In the dynamic process, the actual value of i_{sq} can

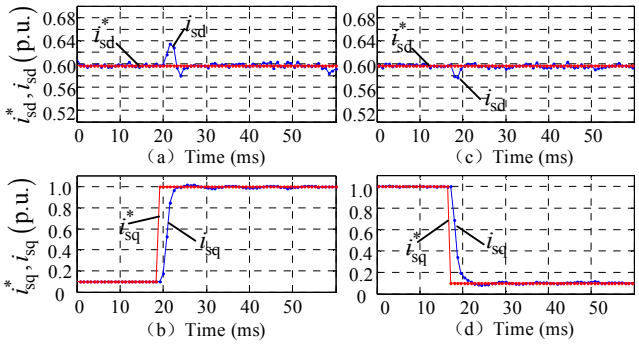

Fig. `5. (a) Reference and actual values of d-axis current when q-axis current step-up, (b) Reference and actual values of q-axis current when q-axis current step-up, (c) Reference and actual values of d-axis current when q-axis current step-down, (d) Reference and actual values of d-axis current when q-axis current step-down.

track the reference value within 2ms. In addition, d-axis current coupling disturbance will appear when q-axis current steps, but the disturbance amplitude (about 0.05p.u.) and time (about 3ms) are small.

C. *Speed control mode*

Fig.6 presents the q axis current response to speed steps. The motor speed steps between 0.06(p.u.) and 0.6(p.u.) with 1(p.u.) load torque. The waveforms show that q-axis current can track reference value quickly without overshoot and oscillation. The periodic fluctuation of q-axis current in low speed is produced by the fluctuation of resistance torque, which is caused by the inaccurate alignment of the experimental system. However, the speed is stable and no obvious fluctuation, which indicates that the system has excellent ability to resist load disturbance.

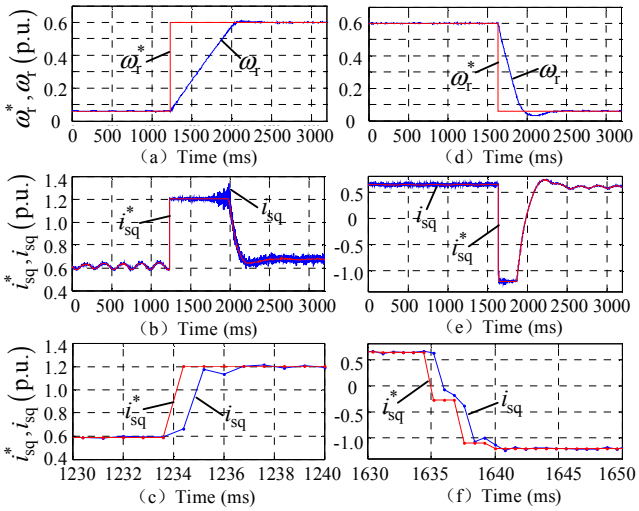

Fig. 6. (a) Reference and actual values of motor speed when speed step-up, (b) Reference and actual values of q-axis current, (c) Details of q-axis current when speed step-up, (d) Reference and actual values of motor speed when speed step-down, (e) Reference and actual values of q-axis current, (f) Details of q-axis current when speed step-down.

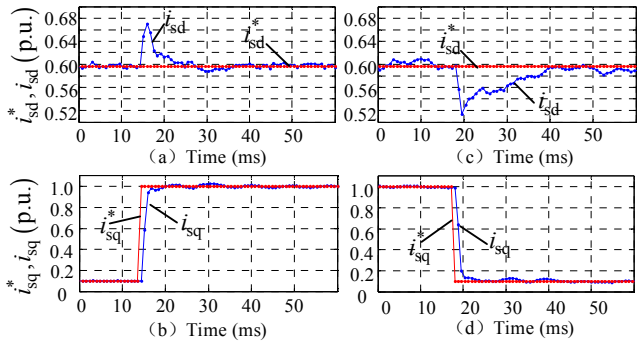

Fig. `7. (a) Reference and actual values of d-axis current when q-axis current step-up, (b) Reference and actual values of q-axis current when q-axis current step-up, (c) Reference and actual values of d-axis current when q-axis current step-down, (d) Reference and actual values of d-axis current when q-axis current step-down.

D. *Comparison with the PI regulator*

Fig. 7 presents the waveform of the d-axis and the q-axis current when the PI regulator is used. The proportional and integral coefficients of the PI regulator are both taken 0.8. In the dynamic process, the actual value of i_{sq} can track the reference value within 1.4ms, which is faster than the MPC. However, the d-axis current coupling disturbance is worse than MPC. Without considering the effect of the one-step delay may be the reason that causes the dynamic response of MPC to slow down.

V. CONCLUSIONS

This paper studies the current control method of an IM based on CCS-MPC. The control method takes advantage of the ability of MPC to deal with the MIMO system, replaces the two PI current regulators used in traditional vector control by MPC regulator, and realizes the unified control of d-axis and q-axis current. In addition, the method applies augmented models to achieve offset-free tracking; adopts Hildreth's QP procedure to realize the online optimization for the time-varying system with constraints. A tuning method for the prediction horizon length and weighting coefficients of cost functions based on the poles distribution of the closed-loop system is also presented in the paper.

REFERENCES

[1] J. Rodriguez and P. Cortes, *predictive control of power converters and electrical drives*. Chichester, UK: John Wiley & Sons, Ltd, 2012.

[2] J. Rodriguez, M. P. Kazmierkowski, J. R. Espinoza, P. Zanchetta, H. Abu-Rub, H. A. Young, and C. A. Rojas, "State of the Art of Finite Control Set Model Predictive Control in Power Electronics," *Industrial Informatics, IEEE Transactions on,* vol. 9, pp. 1003-1016, May 2013.

[3] P. Cortes, M. P. Kazmierkowski, R. M. Kennel, D. E. Quevedo, and J. Rodriguez, "Predictive Control in Power Electronics and Drives," *Industrial Electronics, IEEE Transactions on,* vol. 55, pp. 4312-4324, Dec 2008.

[4] S. Mariethoz, A. Domahidi and M. Morari, "High-Bandwidth Explicit Model Predictive Control of Electrical Drives," *Industry Applications, IEEE Transactions on,* vol. 48, pp. 1980-1992, Dec 2012.

[5] F. Morel, L. Xuefang, J. M. Retif, B. Allard, and C. Buttay, "A Comparative Study of Predictive Current Control Schemes for a Permanent-Magnet Synchronous Machine Drive," *Industrial Electronics, IEEE Transactions on,* vol. 56, pp. 2715-2728, July 2009.

[6] W. Liuping, *Model predictive control system design and implementation using Matlab*: Springer London, 2009.

[7] A. Linder and R. Kennel, "Model Predictive Control for Electrical Drives," in *Power Electronics Specialists Conference, 2005. PESC '05. IEEE 36th*, Recife, 2005, pp. 1793-1799.

[8] S. Mariéthoz and M. Morari, "Explicit Model-Predictive Control of a PWM Inverter With an LCL Filter," *IEEE Transactions on Industrial Electronics,* vol. 56, pp. 389-399, Feb 2009.

[9] S. Bolognani, R. Kennel, S. Kuehl, and G. Paccagnella, "Speed and current Model Predictive Control of an IPM synchronous motor drive," in *Electric Machines & Drives Conference (IEMDC), 2011 IEEE International*, 2011, pp. 1597-1602.

[10] S. Kouro, P. Cortés, R. Vargas, U. Ammann, and J. Rodríguez, "Model Predictive Control-A Simple and Powerful Method to Control Power Converters," *IEEE Transactions on Industrial Electronics,* vol. 56, pp. 1826-1838, June 2009.

[11] W. Liuping, C. Shan, D. Yoo, L. Gan, and K. Ng, *PID and predictive control of electrical drives and power converters using Matlab Simulink*: John Wiley & Sons Singapore Pte. Ltd, 2015.

[12] C. Shan, W. Liuping and E. Rogers, "Model Predictive Control of a Permanent Magnet Synchronous Motor," in *IECON 2011 - 37th Annual Conference on IEEE Industrial Electronics Society*, 2011, pp. 1928-1933.